Low-Thrust LO_2/LH_2 Engine Performance with a 300:1 Nozzle

H. Miyajima* and K. Nakahashi†
National Aerospace Laboratory, Miyagi, Japan
H. Hirakoso‡
Mitsubishi Heavy Industries, Ltd., Nagoya, Japan
and E. Sogame§
National Space Development Agency of Japan, Tokyo, Japan

Altitude simulation tests for a thrust chamber with a 300:1 area ratio nozzle were conducted to evaluate the performance potential of a hydrogen/oxygen propellant system with a 4200 N (943 lbf) thrust level and a chamber pressure of 3.5 MPa (507 psia). The thrust chamber consisted of a channel wall combustion chamber with a brazed copper powder close out and a dump/film cooled nozzle extension. Measured specific impulses were compared with numerical predictions. There was reasonable agreement between observed and predicted performances. A specific impulse of 458 s was obtained at a chamber mixture ratio of 5.0 for an injector with 98% c^* efficiency. An apparent effect of unburned propellant reaction in the nozzle for the less efficient injector was observed. A new method for fabrication of a combustion chamber and the effect of film cooling by the dumped hydrogen are also described briefly.

Nomenclature

AR = local area ratio
c^* = characteristic velocity
C_{Fv} = vacuum thrust coefficient
g = gravitational acceleration
I_{spv} = vacuum specific impulse
I_s = secondary flow vacuum specific impulse
$\dot{m}$ = mass flow rate
$\dot{m}_{cf}$ = fuel mass flow rate of main flow
MR = mixture ratio
P_c = chamber pressure
q_w = wall heat flux
T_{HJ} = hydrogen temperature supplied to the injector
ϵ = overall area ratio
η = efficiency

Subscripts

c = chamber or main flow
E = engine
s = secondary flow

Introduction

THE low-thrust oxygen/hydrogen propulsion system is one of the attractive candidates for the upper stages of launch vehicles,[1,2] and orbit transfer vehicles for large space structures.[3,4] Although extensive system analyses for these applications have been conducted, the performances of very large area ratio nozzles, such as proposed in those analyses, have not been demonstrated.

The authors have gathered nozzle performance data up to an area ratio of 140: 1 in support of the development of Japan's first oxygen/hydrogen rocket engine, the LE-5.[5] These data also were used for the evaluation of a numerical performance prediction method. The prediction method, modeled after JANNAF methodology, included a finite difference procedure developed by Nakahashi et al.[6] for the calculation of two-dimensional kinetic flow.

The present experimental study provides an extended data base to a nozzle area ratio of 300:1. Delivered specific impulses were compared with numerical predictions. The vacuum thrust level was 4200 N (943 lbf) at a chamber pressure of a 3.5 MPa (507 psia). A channel walled combustion chamber fabricated by a new method was used. A combined dump/film cooled nozzle extension was attached to the chamber. The method of fabrication for the chamber and the effect of supersonic film cooling by the dumped hydrogen will also be described briefly.

Test Facility and Test Article

Test Facility

All of the experiments presented herein were conducted at the National Aerospace Laboratory's high-altitude test facility for rocket engines.[7] Liquid hydrogen and liquid oxygen propellant supply systems and a 0.65-m inlet diameter supersonic diffuser were added to the original facility. The thrust chamber was mounted on a thrust measuring system in the capsule. An exhaust sytem consisting of a diffuser and a two-stage steam ejector evacuated the capsule to about 0.32 kPa (2.4 Torr) at steady states.

Test Hardware

The thruster assembly used is shown in Fig. 1. Nominal operating conditions are shown in Table 1 along with the estimated precision of measured parameters (to be discussed later). The nominal vacuum thrust was 4188 N (941 lbf) at a chamber pressure of 3.48 MPa (505 psia). The overall nozzle area ratio was 300:1.

The injector had 18 coaxial elements, a central torch igniter hot gas port, and a flat Regimesh face with 12 peripheral film coolant orifices as shown in Fig. 2. The injector element was designed so that it had an injection velocity ratio of 15:1 at a hydrogen temperature of 120 K. The inner diameter of the liquid oxygen tube was 1.66 mm and the annualar cross-sectional area of the hydrogen injection was 4.6 mm.[2] The hydrogen tube diverged by a 34-deg half-angle 2 mm long to the injector face. The oxygen tube was recessed 1.7 mm from the corner of the divergence. Injector film coolant flow was

Received April 22, 1983; presented as Paper 83-1313 at the AIAA 19th Joint Propulsion Conference, Seattle, Wash., June 27-29, 1983; revision received Jan. 7, 1984.

*Chief, Rocket Altitude Performance Section. Member AIAA.
†Research Scientist, Kakuda Branch. Member AIAA.
‡Manager, Liquid Rocket Engine Section.
§Senior Engineer, Propulsion Development Group.

approximately 4.6% of the hydrogen supplied to the injector. In the later part of this program, the film coolant orifices were plugged by welding to improve the chamber energy release efficiency.

The inner dimensions of the combustion chamber are shown in Fig. 1. The diameter of the cylindrical portion was 6.6 cm and the throat diameter was 2.8 cm. The characteristic length L^* was 73 cm. The copper liner of the combustion chamber had 40 slotted cooling channels. These channels were closed out with a copper powder/brazing material composite layer which also bonded a stainless steel (CRES) outer shell. The layer was approximately 2 mm thick. The method of fabrication will be described later. For reference and emergency cutoff, a thermocouple was embedded in the copper liner at the throat section about 1 mm from the inner surface.

The combustion chamber section was terminated at the local nozzle area ratio AR = 8. The nozzle extension consisted of a dump cooled section from AR = 8 to 80 and a film cooled section from AR = 80 to 300. The dump cooled section was of a double-walled design with 90 axial cooling channels slotted in the nickel liner covered with a CRES outer shell. Attached at the downstream end of each channel were small supersonic nozzles with an area ratio of 11:1. The dump nozzle area ratio was selected so that the static pressure of the main flow and dumped gas was approximately the same at the dumped hydrogen flow rate of 7% of the fuel supplied to the injector. Five pairs of thermocouples were equipped to measure the axial variation of the coolant and nickel liner temperatures. The dumped hydrogen at the main nozzle area ratio AR = 80 served as film coolant to the downstream nozzle wall. The film cooled nozzle extension was made from CRES about 2 mm thick. Five thermocouples were attached to the outer surface of the nozzle at different axial locations. The nozzle wall static pressure was measured at 19 axial locations.

Chamber Fabrication

Since the fabrication method of the slotted cooling channel combustion chamber applied here apparently has not been tried elsewhere, some comments on the fabrication method are in order.

The feature of this new method is that the close out of the cooling channel and the bonding of the liner to the outer shell can be performed simultaneously by melting brazing material and allowing it to flow into the pores of the gap which are packed with fine copper powder. The geometrically complex gap is formed between the outer shell and the inner liner with milled cooling channels which are filled with removable ceramics. The method is tentatively called the "powder/melt infiltration" process.

Preliminary specimen tests were conducted to determine the tensile strength of the silver brazed copper powder composite material. The measured tensile strength is shown in Table 2. The tensile strength of the composite was about 290 N/mm^2 (42 ksi) and it was higher than that of the copper liner material (oxygen-free high-conductivity copper, OFHC) i.e., 206 N/mm^2 (30 ksi). A tension test result (Fig. 3) shows clearly that the tensile strengths of the composite and the bonded interface between the composite and the copper were greater than that of the copper.

The above encouraging result led to the use of this composite for the close out of the cooling slots and, simultaneously, bonding the liner to the outer shell. Figure 4 illustrates the fabrication processes of the chamber. In the second process, the channels were filled with alumina mixed with potassium phosphate binder and then baked at an appropriate temperature. The gap between the liner and outer shell was set to about 2 mm and was packed with 80-100 mesh OFHC powder. The powder filled liner-outer shell assembly was set vertically in a vacuum furnace and the brazing material was put on a reservoir on top of the assembly. Melted brazing material flowed down and filled the pores by surface tension. After a close out/bonding process, the alumina core was removed by hot water flushing. Finally, the usual machining and welding processes were followed to complete the fabrication of a combustion chamber.

The major advantage of this "powder/melt infiltration" process is that the close out/bonding for complex geometry can be done in a short time with a conventional vacuum furnace.

Test Results

Estimated Precision of Performance Parameters

Measured vacuum specific impulse variation within a run was about 0.5 s after 10 s of firing, although it took about 25 s to attain a steady temperature distribution in the dump nozzle. The film cooled wall temperature did not reach steady state within 50 s of firing duration. The firing duration was limited to 50 s due to the capacity of the liquid oxygen tank. Primary data were recorded at a sampling rate of 100 Hz/channel. For consistency, the average of 100 data during 39-40 s after ignition were used for the performance calcu-

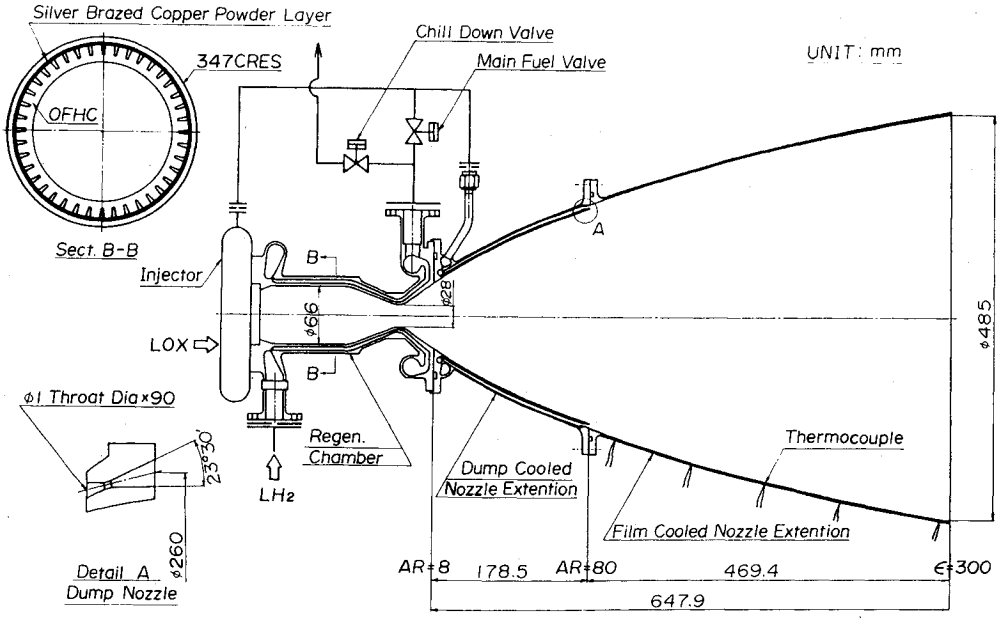

Fig. 1 300:1 area ratio thruster.

lation, except for a few initial runs where firing duration was set to 30 s.

Estimated precision of the performance parameters and that of the pertinent measured parameters are summarized in Table 1. It is recognized that certain parameters are critical for determining thruster performance, i.e., thrust, chamber pressure, and mass flow rate of oxygen. It was found that for very large area ratio nozzles, otherwise negligible capsule pressure precision had a sizable effect on the overall precision of specific impulse. For this reason, chamber pressure, oxygen mass flow, and capsule pressure were measured redundantly. Since we lacked adequate end-to-end calibration of the cryogenic volume flow rate, the precision of turbine flowmeters was adopted as ±1% (specified by the manufacturers). As shown in Table 1, the estimated precision of vacuum specific impulse was within ±1.1%.

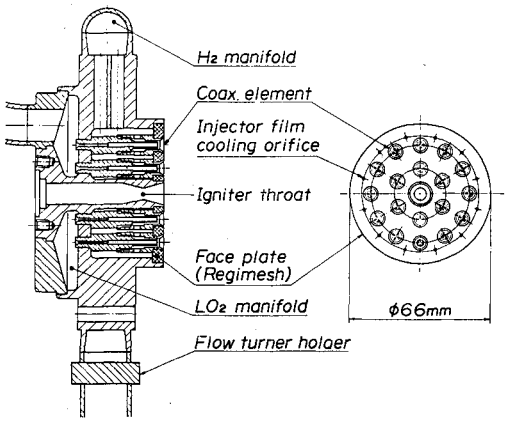

Fig. 2 Sketch of injector.

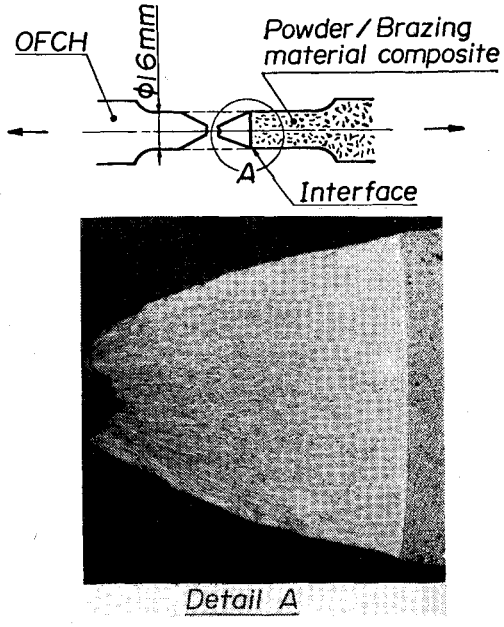

Fig. 3 Result of tension test of bonded specimen.

Thrust Chamber Performance

Figure 5 shows the experimental delivered engine vacuum specific impulse $I_{spv,E}$ as a function of engine mixture ratio MR_E. The unit of specific impulse is N-s/kg, but in the following discussion it is divided by the gravitational acceleration g for convenience. These data were obtained with different dump coolant flow rates, as indicated as a percentage of the main chamber hydrogen flow rate. Data points with a closed symbol, designated injector 3′, were obtained from injector 3 with plugged film coolant orifices; the injector film coolant flow being reduced to zero from approximately 4.6% of the hydrogen supplied to the injector. It can be seen that vacuum specific impulse decreases rather drastically with mixture ratio. The effect of dump coolant flow rate apparently was buried in the run-to-run reproducibility of the data.

In order to evaluate the chamber and nozzle efficiency, it is necessary to eliminate the dump coolant contribution from engine specific impulse. To estimate the effective vacuum specific impulse of the dumped gas, the method developed by Stromsta and Hosack[8] was employed.

It was found that dump coolant vacuum specific impulse was dictated by the dumped hydrogen temperature and was within a range of 360 to 430 s.

Table 1 Nominal operating condition and estimated precision

Item	Nominal value	Precision % of nominal
Capsule pressure, KPa	0.32	12.5
Vacuum thrust, N	4188	0.4
Engine specific impulse, s	455	1.0
Engine mixture ratio	5.0	2.13
LO_2 mass flow rate, g/s	782	1.04
LH_2 mass flow rate, g/s	156	1.86
Dump coolant mass flow rate, g/s	9.8	3.0
Chamber pr. (stag.) MPa	3.48	0.21
Chamber mixture ratio	5.35	2.13
Characteristic velocity, c^*, m/s	2300	0.96
c^* efficiency	0.981	1.03
Main flow thrust coefficient	1.944	0.48
Main flow specific impulse, s	456	1.07

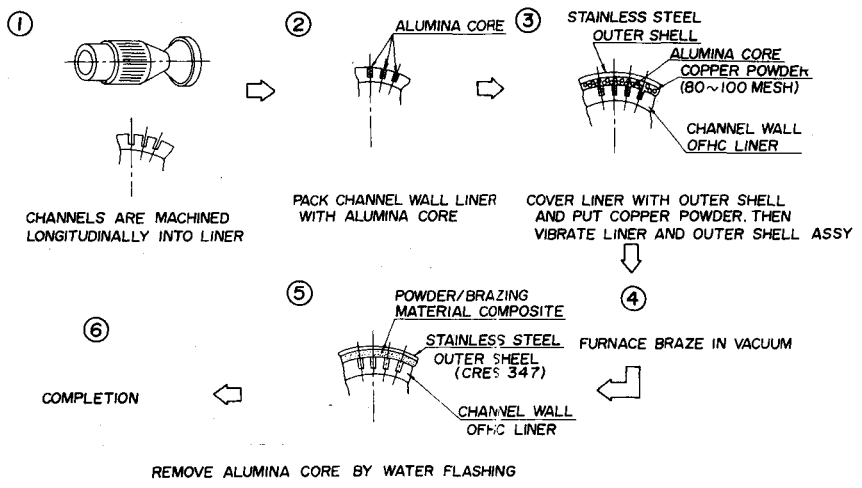

Fig. 4 Fabrication process of power/melt infiltration method.

Once the effective specific impulse of the dumped hydrogen is determined, the main flow vacuum specific impulse $I_{spv,c}$ may be calculated from

$$I_{spv,E}=\frac{\dot{m}_c I_{spv,c}+\dot{m}_s I_s}{\dot{m}_c+\dot{m}_s}$$

Chamber characteristic velocity c^* is related to main flow specific impulse $I_{spv,c}$ through the main flow vacuum thrust coefficient C_{Fv} as

$$I_{spv,c}=c^* C_{Fv}$$

Figure 6 shows the three performance parameters of the main flow as a function of the chamber mixture ratio MR_c. For comparison, also shown are the data obtained for area ratio $\epsilon=140$ with a water cooled thruster, i.e., nozzle and combustion chamber both cooled by water.[5] The injector used (injector 2) was of the same design as that used in this program. The characteristic velocity of the water cooled chamber was about 0.8% smaller than that of the regeneratively cooled chamber. Although the difference was within the precision listed in Table 1, it seems that unknown factors are involved in the consistent difference. Characteristic velocity increased by about 1.5% when the injector film coolant orifices were plugged by welding injectors 3′ and 3 (see Fig. 7 also).

From comparison of data obtained using an injector of the same design (injectors 2 and 3), it seems that an increase in nozzle area ratio from 140 to 300 corresponded to a specific impulse increase of more than 10 s. However, when corrected for the chamber energy release efficiency difference, approximated by characteristic velocity efficiency difference, the increase was 7 to 6 s in a mixture ratio range of 5 to 6. An increase of about 8.6 s was predicted by numerical methods to be described later. In this paper, the term chamber energy release efficiency is used to designate the overall energy release efficiency of the chamber in accordance with c^* efficiency.

An interesting observation is that the C_{Fv} for the better performing injector (injector 3′) was clearly lower than that of the original injector (injector 3) at the same overall area ratio $\epsilon=300$. To illustrate this effect, performance efficiencies of injectors 3′ and 3 are compared in Fig. 7. The c^* efficiency of injector 3′ was 1.5% higher than that of injector 3 and C_{Fv} efficiency 0.5% lower, resulting in 1% higher I_{sp} efficiency averaged over the range of tests. It should be noted that for a c^* efficiency range of 96-98%, the increase of c^* efficiency does not translate to I_{sp} efficiency. The same trend was observed earlier with a water cooled thrust chamber in which c^* efficiency was varied by changing the hydrogen temperature supplied to the injector.[5] This trend may be attributed to the combined effect of chamber energy release loss and the nozzle expansion process, i.e., the effect of additional reaction

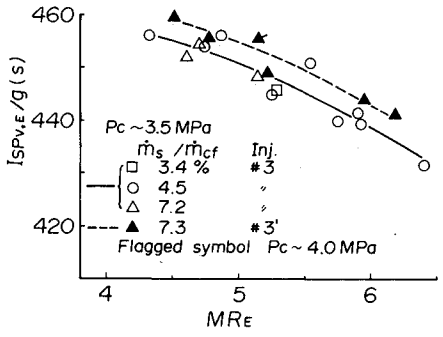

Fig. 5 Delivered specific impulses vs engine mixture ratio.

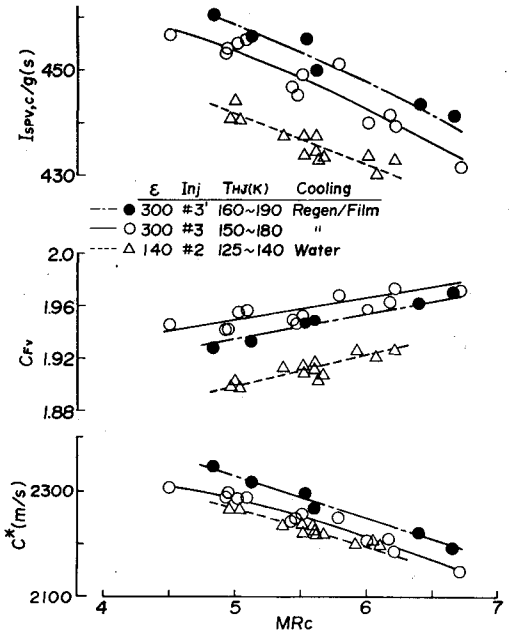

Fig. 6 Chamber performance parameters.

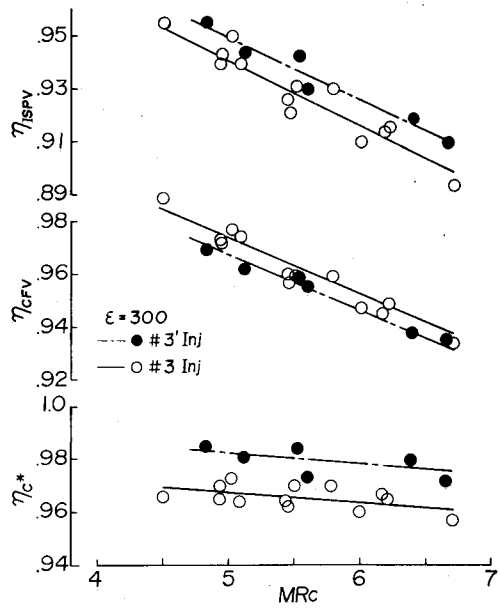

Fig. 7 Comparison of performance efficiencies for two injectors.

Table 2 Tensile strength of copper powder/brazing material composite

Test piece no.	Diameter, mm	Load, N	Tensile strength, N/mm^2	Elongation, %	Contraction of area, %
1	7.60	12,900	284	21.5	22.7
2	8.03	14,760	291	21.8	23.4
3	6.96	11,770	309	22.0	25.6

Table 3 Computer codes used

Code	Source	Ref.
ODE	NASA Lewis	11
ODK	NAL	6
TDK	NAL	6
TBL	JANNAF	13

during the nozzle expansion of propellants which failed to react in the combustion chamber.

Film Cooling by Dumped Hydrogen

As stated earlier, the outer wall temperatures measured on the five axial stations of the film cooled section of the nozzle extension did not attain steady states during 50 s of firing duration. An approximate method was used to obtain wall heat flux from the measured outer wall temperatures. Since the Biot number in the film cooled nozzle was not larger than 0.01, the nozzle wall is assumed to be thermally thin; i.e., a temperature gradient perpendicular to the surface is negligible. It is also assumed that the outer wall is effectively isolated by the low-pressure environment and that the temperature gradient along the wall is also negligible. With these simplifying assumptions, the heat flux can be calculated easily from the timewise variation of the outer wall temperature. Measured wall temperatures increased with time nearly linearly during the initial 20 s followed by a continuously decreasing slope. In spite of the fact that the dumped gas temperature was still increasing, heat fluxes were calculated at 20 s in favor of the approximate linear behavior of the wall temperature and a relatively small radiation correction for the low wall temperatures (less than 600 K).

Figure 8 shows some of the results of wall heat fluxes for two different flow rates as a function of local area ratio AR. Also included in this figure are measured and predicted heat fluxes for smooth nozzles of an overall area ratio $\epsilon = 140$. Thin film heat flux meters were used for the heat sink nozzle and a calorimetric technique was used for the water cooled nozzle with circumferential semilocal coolant passages. The film cooled nozzle used in this program had a sudden enlargement just downstream of AR = 80 where supersonic secondary flow was injected tangentially through 90 dump nozzles (see Fig. 1). Since no simple method for predicting the heat transfer in this flowfield was available, a calculated curve for $\epsilon = 300$ was obtained for a smoothed contour without the film coolant injection step using the turbulent boundary-layer code listed in Table 3. It can be seen that the effectiveness of the supersonic film cooling by the dumped hydrogen was significant and it persisted further downstream at least to about AR = 200.

Chamber Condition after Firings

Twenty-two firing tests with accumulated duration of 775 s were run with the first combustion chamber fabricated by the powder/melt infiltration method. The range of pressure difference between the cooling channel and cylindrical chamber section was 1.5-2.1 MPa (218-305 psi) and that at the exit of chamber section was 4.0-4.6 MPa (580-667 psi). The nozzle throat wall temperatures measured at about 1 mm from the inner wall were 420-530 K.

No measurable nozzle throat diameter change was observed during this test series. It is known that a substantial separation of the liner from the outer shell in the vicinity of the throat leads to a drastic reduction of the throat diameter.[9]

To check the possibility of spreading structural defect from a bubble which would be formed if the brazing material failed to infiltrate to a small volume, 12 leak check holes and a circumferential slot reaching to the copper/brazing material composite layer were provided on the cylindrical portion of the outer shell. No leak was detected during and after the test series.

In short, a combustion chamber fabricated by this new method seems to have sufficient durability for the scale and operating conditions of the present study.

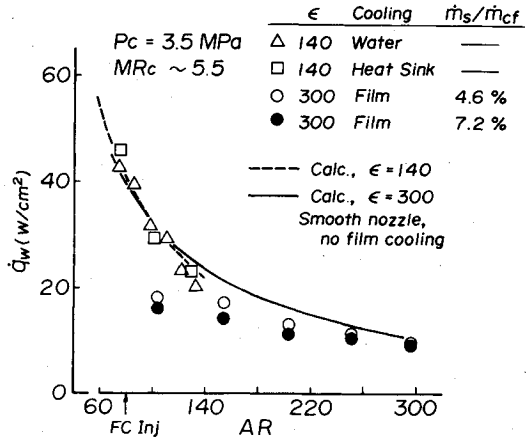

Fig. 8 Effect of film cooling by dumped hydrogen.

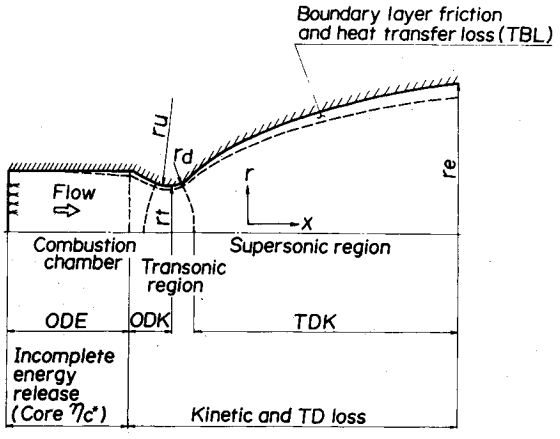

Fig. 9 Simplified flow model for nozzle performance prediction.

Comparison of I_{sp} with Prediction

Method of Prediction

The flow model employed in this study is a simplified version of the JANNAF methodology[10] as shown in Fig. 9. Streamtube to streamtube mixture ratio variations were not taken into account. Although combustion chamber energy release efficiency simulation was attempted by assigning reduced enthalpies to propellants injected into the chamber so that calculated c^* efficiencies coincide with measured ones, resulting calculated delivered specific impulses were much lower than those measured. Therefore, chamber energy release efficiency was simply approximated by the measured c^* efficiency. Figure 9 shows the associated losses and flow subdivisions used for computation. (ODE = one-dimensional equilibrium flow, ODK = one-dimensional kinetic flow, TDK = two-dimensional kinetic flow, and TBL = turbulent boundary-layer flow. The same abbreviations are used for the computer codes of the corresponding flow.)

The computer codes used are summarized in Table 3. For the calculation of one-dimensional equilibrium flow, NASA's code[11] was used, while the code for a one-dimensional kinetic flow was newly developed.[6] For the calculation of transonic flow, the analytical solution obtained by Kliegel and Levine[12] was used. A finite difference procedure with a shock-

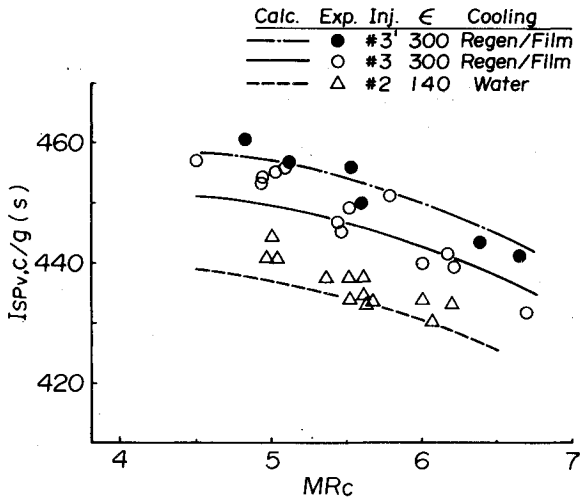

Fig. 10 Comparison of experimental and predicted specific impulse.

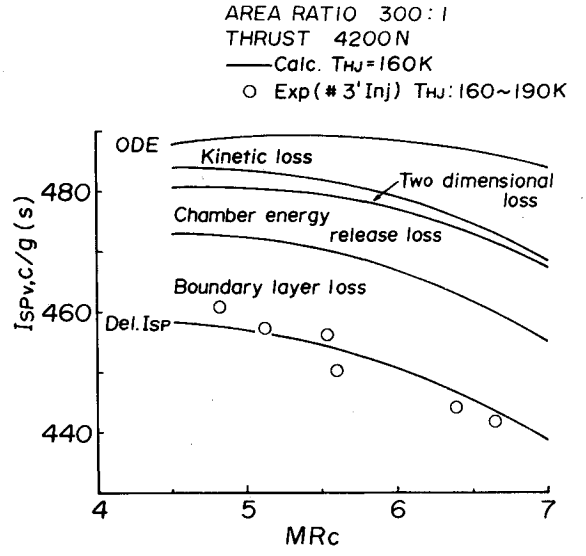

Fig. 11 Specific impulse loss distribution.

capturing concept was adopted[6] for the calculation of two-dimensional kinetic flow. JANNAF's turbulent boundary-layer flow code[13] was used for the calculation of boundary-layer loss.

Comparison of Measured I_{sp} with Prediction

A comparison of calculated and experimental delivered specific impulses is shown in Fig. 10. The experimental data were replotted from Fig.. 6. Calculated delivered specific impulses were not affected greatly by the injector input temperature (a 1.3 s increase was calculated for the increase of temperature from 140 to 180 K). Therefore, over the range of mixture ratios tested, constant input temperatures were used for the calculation; 140 K for area ratio $\epsilon = 140$ configuration corresponding to experimental input, and 160 K for $\epsilon = 300$ configuration. From Fig. 10, it may be seen that the specific impulses for the $\epsilon = 140$ configuration in which c^* efficiencies were between 95.5 and 96% are generally higher than the calculated curve. The data points for injector 3 with the $\epsilon = 300$ nozzle are higher than the calculated curve in the lower mixture ratios and lower in the higher mixture ratios. For the best performing injector used here, about 98% c^* efficiency for injector 3', the agreement between predicted and experimental I_{sp} is much better, although the same trend as in injector 3 may be seen.

In view of the overall experimental precision (1.1%), it may be concluded that the prediction method employed here gives satisfactory results. For cases where chamber energy release efficiency is not sufficiently close to 100%, it seems necessary to consider the effect of delayed reaction in the nozzle of propellants which failed to react in the chamber. This problem has been treated in some detail.[14,15] An effort to incorporate this effect in the prediction method may not be warranted until more accurate data can be obtained.

Figure 11 shows loss distribution among processes for a thruster with an $\epsilon = 300$ nozzle. The boundary-layer loss was the greatest among losses for the configuration and operating condition; therefore, it is important to assess the boundary layer loss in more detail. The reason that the delivered I_{sp} decreased rather drastically with an increase of mixture ratio can be attributed mainly to kinetic loss and, to a lesser degree, to the chamber energy release loss. The predicted results show that even if a perfect chamber energy release could be achieved, it would be difficult to obtain more than 464 s main flow specific impulse at MR = 5.5 for this particular configuration.

Conclusions

Altitude simulation tests of a liquid oxygen/liquid hydrogen thrust chamber with a 300:1 area ratio nozzle were conducted at a 4200 N (943 lbf) thrust level and a chamber pressure of 3.5 MPa (507) psia. A channel wall combustion chamber fabricated by a new method was used. The results are summarized as follows.

1) A main flow vacuum specific impulse of 458 s was obtained at a chamber mixture ratio of 5.0 for c^* efficiency of 98%.

2) Delivered specific impulse decreased rather drastically with an increase of mixture ratio mainly due to kinetic losses.

3) Numerical prediction of delivered specific impulse was reasonable.

4) In a c^*-efficiency range of 96 to 98%, the increase of c^* efficiency does not translate to an I_{sp} increase, presumably because of the delayed reaction of the unburned propellant in the nozzle.

5) Effectiveness of supersonic film cooling by dumped hydrogen at an area ratio 80:1 was significant.

6) A channel wall combustion chamber fabricated by the "powder/melt infiltration" technique accumulated 775 s of firing duration with 22 starts without a defect.

More accurate experimental data in a wider range, as well as continued efforts to improve the prediction method, would be required to fully understand the processes occurring in a low-thrust, large area ratio thruster.

Acknowledgments

The authors express their gratitude to Dr. Akio Suzuki, Director of NAL Kakuda, whose support and encouragement were essential to this program. Dr. Masayuki Niino's valuable suggestions regarding the design and testing of a regeneratively cooled chamber are gratefully acknowledged.

References

[1]Kayama, A. et al., "Feasibility Study of 3rd Stage LOX/LH2 Engine System," *Proceedings of the 13th International Symposium on Space Science and Technology,* Tokyo, 1982, pp. 259-264.

[2]Kayama, A. et al., "LOX/LH2 Propulsion System for Launch Vehicle Upper Stage," *Proceedings of the 13th International Symposium on Space Science and Technology,* Tokyo, 1982, pp. 265-273.

[3]Christensen, K. L. and Mellish, J. L., "Liquid Rocket Engine Technology for Orbit Transfer Vehicles," AIAA Paper 81-1458, 1981.

[4]Shoji, J. M., "Low Thrust Chemical Propulsion for Large Space Structure Orbit Transfer," AIAA Paper 81-1459, 1981.

[5]Miyajima, H. et al., "Performance of a Small LO2/H2 Thrust Chamber with High Area Ratio Nozzles," *Proceedings of the 13th*

International Symposium on Space Science and Technology, Tokyo, 1982, pp. 253-258.

[6]Nakahashi, K., Miyajima, H., Kisara, K., and Moro, A., "Prediction Method of Rocket Nozzle Performance," National Aerospace Lab., NAL TR-771, 1983.

[7]"High Altitude Test Facility for Rocket Engine at N.A.L.," National Aerospace Lab., NAL TR-454, 1976.

[8]Stromsta, R. R. and Hosack, G. A., "Analytical Methods for Computing the Effectss of Turbine Exhaust and Film-Coolant Injection on Rocket Engine Performance," AIAA Paper 69-473, 1969.

[9]Yatsuyanagi, N. et al., "A Study of Liquid Hydrogen Cooled LO2/LH2 Rocket Combuster with Slotted Wall Liner," National Aerospace Lab., NAL TR-697, 1981.

[10]Powell, W. B., "Current Status of the ICRPG Liquid Propellant Thrust Chamber Performance Evaluation Methodology," AIAA Paper 69-468, 1969.

[11]Gordon, S. and McBride, B. J., "Computer Program for Calculation of Complex Chemical Equilibrium Compositions, Rocket Performance, Incident and Reflected Shocks, and Chapman-Jouget Detonations," NASA SP-273, 1971.

[12]Kliegel, J. R. and Levine, J. N., "Transonic Flow in Small Throat Radius of Curvature Nozzles," *AIAA Journal,* Vol. 7, July 1969, pp. 1375-1378.

[13]Omori, S., Gross, K. W., and Krebsbach, A., "Wall Temperature Distribution Calculation of a Rocket Nozzle Contour," NASA TN D-6825, 1972.

[14]Adams, D. M., "Theoretical Assessment of Some Combustion and Expansion Problem in Rocket Motors," *Journal of Spacecraft and Rockets,* Vol. 5, Feb. 1968, pp. 173-178.

[15]Branch, M. C. and Sawyer, R. F., "Nonequilibrium Combustion and Nozzle Flow in Propellant Performance," *Journal of Spacecraft and Rockets,* Vol. 6, Nov. 1969, pp. 1322-1325.